ESAIM: M2AN 56 (2022) 943–967
https://doi.org/10.1051/m2an/2022023

ESAIM: Mathematical Modelling and Numerical Analysis
www.esaim-m2an.org

NEW FORMULATIONS AND CONVERGENCE ANALYSIS FOR REDUCED TRACER MASS FRAGMENTATION MODEL: AN APPLICATION TO DEPOLYMERIZATION

Mehakpreet Singh[1,2,*], Gavin Walker[1] and Vivek Randade[1]

Abstract. In this work, two discrete formulations based on the finite volume approach for a reduced fragmentation model are developed. The important features such as mass conservation and accurate prediction of the zeroth order moments are accomplished by the modification of the selection function. The new schemes can compute the second order moment, which plays a significant role in predicting the area of the particles in real life applications, with high accuracy without taking any specific measures. A thorough convergence analysis of both schemes including Lipschitz condition and consistency is presented and exhibit second order convergence. The accuracy and efficiency of both schemes is demonstrated by applying them to the depolymerization problem which commonly arises in polymer sciences and chemical engineering. It is demonstrated that the new schemes are easy to implement, computationally efficient and able to compute the numerical results with higher precision even on a coarser grid.

Mathematics Subject Classification. 37N30, 35R09, 80M12.

Received June 17, 2021. Accepted February 18, 2022.

1. Introduction

Several processes like crystallization and granulation where particle size distributions evolve with space and time are widely used in the pharmaceutical industry. Population balance equations are used to track the particles having different properties such as size, shape, porosity, mass and volume. One-dimensional PBEs are routinely used to simulate particle size distributions in crystallization. However, such 1D PBEs do not account for other important properties like tracer mass fractions, liquid content, porosity. Many applications related to the pharmaceutical industry such as sprayed fluidized bed granulator [27,46,47] and twin-screw wet granulator [17] require the information of tracer mass distribution besides particle size. Multi-dimensional PBEs [42,44] have been developed to simultaneously track different intrinsic properties of particles such as tracer mass fraction in addition to particle size distribution. These two PBEs are quite difficult to solve and computationally expensive. Many authors have proposed various numerical techniques in order to solve the complete two dimensional fragmentation equation for tracking a distribution involving two internal properties [31,39] and references therein.

Keywords and phrases. Integro-partial differential equations, finite volume scheme, reduced fragmentation model, convergence analysis, depolymerization.

[1] Bernal Institute, Department of Chemical Sciences, University of Limerick, V94 T9PX Limerick, Ireland.
[2] Bernal Institute, School of Engineering, University of Limerick, Limerick, Ireland.
*Corresponding author: Mehakpreet.Singh@ul.ie

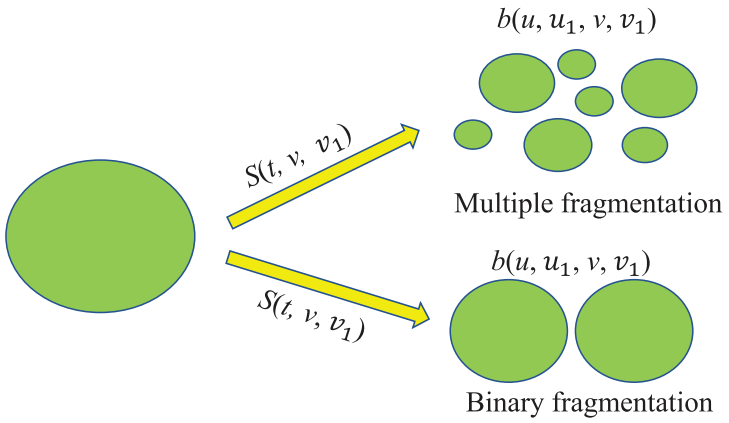

FIGURE 1. Schematic representation of the fragmentation processes in 2D space.

Hounslow *et al.* [14] have reduced a 2D population balance equation to two 1D population balance equations for easing computational demands. There are only few numerical studies are available in the literature which describe the accurate prediction of the tracer mass distribution [14, 23, 33]. The reduced tracer mass fraction equation also has applications in polymer reaction engineering. For example, reduced tracer mass distribution equation for fragmentation process can be used to simulate depolymerization process. It is essential to develop better methods to solve reduced 2D population balance models, particularly to solve reduced tracer mass fraction equations to encourage application of the reduced 2D PBEs to simulate practically relevant systems like granulations [38] and depolymerizations [1]. Such an attempt is presented here.

In this work, our main objective is to develop new methods for solving the reduced tracer mass distribution. For illustrating the methods, a case of a pure fragmentation process is considered in this work. The fragmentation process leads to increase in number of particles and the total mass remains unchanged in the system. The binary and multiple fragmentation processes in two dimensional space having two internal coordinates is depicted in Figure 1. In this work we develop two methods for solving reduced tracer mass fragmentation model.

1.1. Reduced fragmentation model

The complete two dimensional fragmentation equation for tracking the dynamics of number density function corresponding to two internal properties of the particles [5, 9, 40] can be written as

$$\frac{\partial n(t,u,v)}{\partial t} = \int_u^\infty \int_v^\infty S(t,u_1,v_1)b(u,v,u_1,v_1)n(t,u_1,v_1)\mathrm{d}u_1\mathrm{d}v_1 - S(t,u,v)n(t,u,v). \tag{1.1}$$

subject to a initial conditions

$$n(0,u,v) = n_{\mathrm{ini}}(u,v), \tag{1.2}$$

where n, S, and b represent number density function, selection rate and breakage distribution function, respectively. Due to non availability of the experimental technique to extract the complete two dimensional distribution, Hounslow *et al.* [14] developed a reduced model from the complete 2D fragmentation equation by assuming that the fraction of tracer in the fragment remain unchanged during the fragmentation process, that is, $\frac{v_1}{u_1} = \frac{v}{u}$ and the separation of tracer-dependence in b from the size dependence can be done as

$$b(u,v,u_1,v_1) = b(u,u_1)\delta\left(v - \frac{uv_1}{u_1}\right). \tag{1.3}$$

Using the aforementioned notations and relation (1.3), the equation (1.1) can be rewritten as

$$\begin{aligned}\frac{\partial n(t,u,v)}{\partial t} &= \int_u^{\infty}\int_v^{u_1} S(t,u_1)b(u,v,u_1,v_1)n(t,u_1,v_1)\mathrm{d}u_1\mathrm{d}v_1 - S(t,u)n(t,u,v),\\ &= \int_u^{\infty} S(t,u_1)b(u,u_1)n\left(t,u_1,\frac{u_1 v}{u}\right)\frac{u_1}{u}\mathrm{d}u_1 - S(t,u)n(t,u,v). \end{aligned} \tag{1.4}$$

Integrate both side with respect to v from limits 0 to u, then the equation (1.1) can be reformulated to a reduced model for capturing the tracer mass distribution

$$\begin{aligned}\frac{\partial m(t,u)}{\partial t} &= \int_0^u v\int_u^{\infty} S(t,u_1)b(u,u_1)n\left(t,u,\frac{u_1 v}{u}\right)\frac{u_1}{u}\mathrm{d}u_1\mathrm{d}v - \int_0^u vS(t,u)n(t,u,u_1)\mathrm{d}v,\\ &= \int_u^{\infty} S(t,u_1)b(u,u_1)\int_u^{\infty} vn\left(t,u,\frac{u_1 v}{u}\right)\mathrm{d}\left(\frac{u_1 v}{u}\right)\mathrm{d}u_1 - S(t,u)m(t,u)\\ &= \int_u^{\infty} S(t,u_1)b(u,u_1)\frac{u}{u_1}m(t,u_1)\mathrm{d}u_1 - S(t,u)m(t,u). \end{aligned} \tag{1.5}$$

Similarly, the standard equation of 1D fragmentation equation use to track the size distribution function can be also derived who has many real life applications such as twin screw granulation [16], sprayed fluidized bed granulation [19,20] and depolymerization [1]. Different studies including existence and uniqueness [2,12,29,30,36], analytical solutions [21,48,49], numerical methods [4,8,24,25,41,43,45], scattering and self similarity [7,11,13] for standard 1D fragmentation equation can be found in these references. Whereas, the equation (1.5) is handled to capture the tracer mass distribution for high shear granulation [14] and twin screw granulation [38]. The detailed derivation of equation (1.5) is provided in Hounslow *et al.* [14].

1.2. State of the art and motivation

Due to the complex nature of these equations, few numerical methods are available in literature only for solving a fragmentation mass tracer PBE. The first numerical methods to approximate the tracer PBE (1.5) was developed by Hounslow *et al.* [14]. Later, Peglow *et al.* [33] modified the numerical approximation of the Hounslow *et al.* [14]. The major drawback of both numerical methods is that they are highly accurate in predicting the numerical results only for a size independent kernel. Moreover, the other limitation of these methods is related to the grids as these methods can only implemented to specific type of grids. Recently, Kumar *et al.* [23] presented a numerical method for solving a tracer mass aggregation PBE well known as cell average technique which overcome all issues of the existing methods. The idea of cell average is based on finding the average of all new born particles within the cell and then redistribute them to the neighboring nodes in such a way that pre-chosen properties are exactly preserved. This leads to the recalculation of the birth terms which makes this method computationally very expensive.

In addition, the equation (1.5) has been also intensively used for modeling the grinding process [3, 6, 34]. Reid [35] convert the original equation into the cumulative form to solve it analytically for a simpler structured selection function and breakage kernel. In addition, Kapur and Agrawal [18] developed a Cauchy- Picard method for approximating a tracer mass equation whose formulation is very complex. To the best of our knowledge, only few numerical methods are available in the literature for solving a fragmentation mass tracer PBE [14,18,35]. In this work, our aim is propose two new frameworks based on the finite volume scheme (FVS) for approximating a fragmentation mass tracer PBE. The mathematical formulations of these methods are simpler and robust to apply on any kind of grids as well as breakage functions. The new methods have the tendency to predict the integral properties, tracer mass distribution and average size particles with higher precision by consuming lesser CPU time.

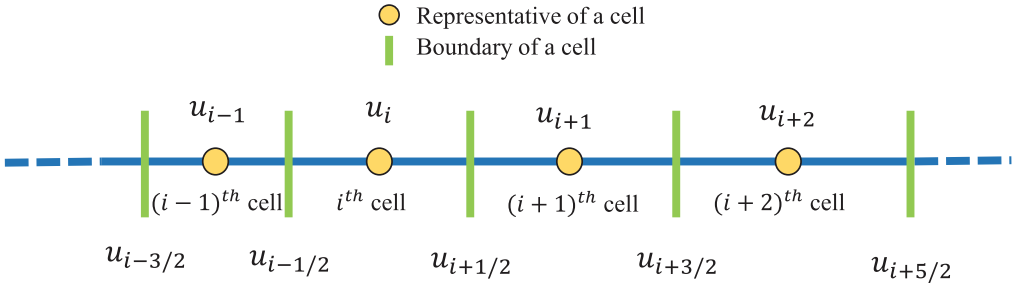

FIGURE 2. Discretization of continuous one dimensional domain.

2. New finite volume approaches

The mathematical derivation of the formulation of the finite volume schemes is began by discretizing the continuous computational domain $[u_{\min}\ u_{\max}]$ into I nonuniform cell as demonstrated in Figure 2. The ith has representative, lower and upper boundaries denoted by u_i, $u_{i-1/2}$ and $u_{i+1/2}$, respectively. Moreover, for the ith cell, step size can be calculated by $\Delta u_i = u_{i+1/2} - u_{i-1/2}$. For the non uniform grids, we denote $\Delta u = \max_i \Delta u_i$, $\delta u = \min_i \delta u_i$, and suppose that there exist a non-negative constant H (independent of the grid considered for discretization) in such a way that

$$\frac{\Delta u}{\delta u} \leq H. \tag{2.1}$$

In order to approximate the integral present in equation (1.5), it is pre-assumed that the particle properties (mass in this case) are accommodated on the representative of each cell, that is,

$$m(t,u) \approx \sum_{j=1}^{I} u_j n_j \delta(u-u_j). \tag{2.2}$$

Suppose that the average value of mass m in ith cell at any time t^n is m_i^p which is the approximation of a function $m(t^p,u_i)$. Further, consider the function m to be sufficiently smooth and can be expanded as $m_i(t) = u_i n(t,u_i)\Delta u_i + \mathcal{O}(\Delta u_i^2)$. The whole idea of the numerical scheme is to obtain set of ODE's by converting the equation (1.5) with integration over the bounds of the ith cell and using the relation (2.2) leads to

$$\frac{\mathrm{d}m_i(t)}{\mathrm{d}t} = B_i(t) - D_i(t), \tag{2.3}$$

with subject to the initial data

$$m_i(0) = \frac{1}{\Delta u_i}\int_{u_{i-1/2}}^{u_{i+1/2}} m(0,u)\mathrm{d}u.$$

Here the particle population corresponding to the birth and death terms are given as

$$B_i(t) = \int_{u_{i-1/2}}^{u_{i+1/2}}\int_{u}^{u_{i+1/2}} b(u,u_1)S(t,u_1)\frac{u}{u_1}m(t,u_1)\mathrm{d}u_1\mathrm{d}u, \tag{2.4}$$

and

$$D_i(t) = \int_{u_{i-1/2}}^{u_{i+1/2}} S(t,u)m(t,u)\mathrm{d}u. \tag{2.5}$$

Let us first simplify the birth term (2.4) by changing the order of integration, we have

$$B_i(t) = \int_{u_{i-1/2}}^{u_{i+1/2}} S(t,u_1)\frac{u}{u_1}m(t,u_1)\int_{u_{i-1/2}}^{u_1} b(u,u_1)\mathrm{d}u\mathrm{d}u_1 + \sum_{k=i+1}^{I}\int_{u_{k-1/2}}^{u_{k+1/2}} S(t,u_1)\frac{u}{u_1}m(t,u_1)\int_{u_{i-1/2}}^{u_{i+1/2}} b(u,u_1)\mathrm{d}u\mathrm{d}u_1.$$

Now use the application of a midpoint quadrature approximation (MDA) on integrals of above equation w.r.t u leads to

$$B_i(t) = S_i m_i \int_{u_{i-1/2}}^{u_i} b(u,u_i)\mathrm{d}u + \sum_{j=i+1}^{I} S_j m_j \int_{u_{j-1/2}}^{u_{j+1/2}} b(u,u_j)\mathrm{d}u + \mathcal{O}(\Delta u^2).$$

Again implement MDA to obtain the discretize form of the death term (2.5) as follows:

$$D_i(t) = S_i m_i + \mathcal{O}(\Delta u^2). \tag{2.6}$$

Further, let us denote the numerical approximation $\hat{m}_i$, then the discrete equations (2.3) can be written as

$$\frac{\mathrm{d}\hat{m}_i}{\mathrm{d}t} = \sum_{j=i}^{I} S_j \hat{m}_j \frac{u_i}{u_j}\eta_{i,j} - S_i\hat{m}_i. \tag{2.7}$$

Here

$$\eta_{i,j} = \int_{u_{i-1/2}}^{\phi_j^i} b(u,u_j)\mathrm{d}u,$$

and ϕ_j^i can be defined as

$$\phi_j^i = \begin{cases} u_i, & \text{when } j = i, \\ u_{i+1/2}, & \text{otherwise.} \end{cases}$$

The above formulation does not satisfy the mass conservation law which is a necessary condition for any numerical method. The numerical scheme holds the mass conservation law when it satisfies the following condition:

$$\frac{\mathrm{d}}{\mathrm{d}t}\sum_{i=1}^{I} m_i = 0. \tag{2.8}$$

For proving the result, take a summation $\sum_{i=1}^{I}$ on both sides the equation (2.7) which gives

$$\frac{\mathrm{d}\sum_{i=1}^{I}\hat{m}_i}{\mathrm{d}t} = \sum_{i=1}^{I}\sum_{j=i}^{I} S_j\frac{u_i}{u_j}\hat{m}_j\eta_{i,j} - \sum_{i=1}^{I} S_i\hat{m}_i. \tag{2.9}$$

Change the order of the first summation, we have

$$\frac{\mathrm{d}\sum_{i=1}^{I}\hat{m}_i}{\mathrm{d}t} = \sum_{j=1}^{I} S_j\hat{m}_j\left(\sum_{i=1}^{j}\frac{u_i}{u_j}\eta_{i,j} - 1\right) \neq 0. \tag{2.10}$$

Hence, the formulation (2.7) do not satisfy the mass conservation law.

In order to show these results, the comparison of normalized moments and number of particles in each cell obtained from the formulation (2.7) are compared numerically and analytically for linear selection function ($S(u) = u$) and binary breakage kernel $\left(b(u,u_1) = \frac{2}{u_1}\right)$. For the comparison, the exponential initial condition $m(0,u) = e^{-u}$ is considered. The computational domain $[10^{-9}\ 200]$ are divided into 30 nonuniform cells and the simulation is run from time 0 to 10.

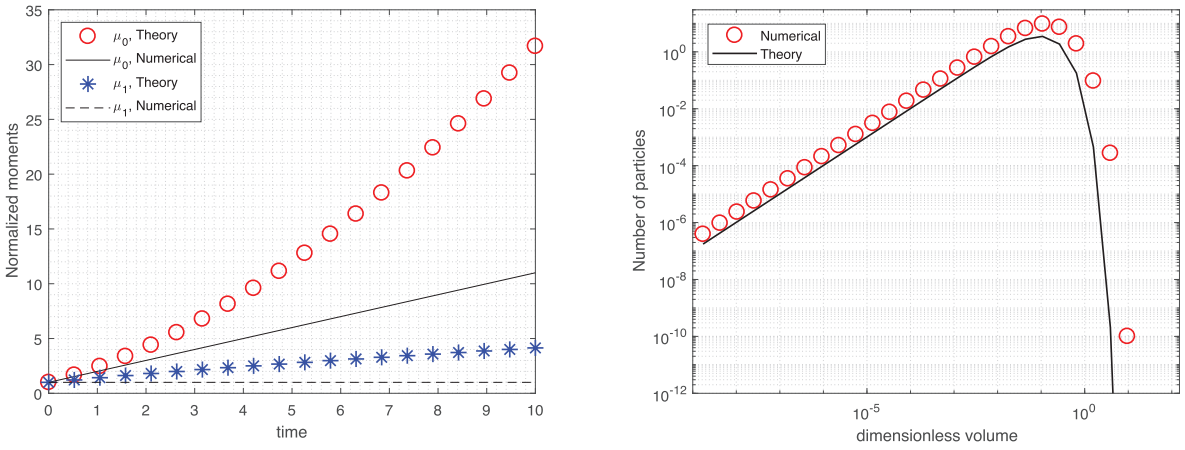

(a) (b)

FIGURE 3. Normalized moments and number of particles using linear selection function and binary breakage kernel obtained from formulation (2.7). (a) Zeroth and first order moments. (b) Number of particles.

2.1. Mass conserving scheme (OOM)

It can be seen that the formulation (2.7) neither conserve the total mass in the system nor predicts the zeroth order moment accurately. In addition, this formulation fails to predict the number of particles in each cell accurately. In order to achieve the mass conservation property, the selection function in the second term of the formulation (2.7) is modified, hence can be read as

$$\frac{\mathrm{d}\hat{m}_i}{\mathrm{d}t} = \sum_{j=i}^{I} S_j \hat{m}_j \frac{u_i}{u_j} \eta_{i,j} - \hat{S}_i \hat{m}_i, \tag{2.11}$$

where

$$\hat{S}_i = \frac{S_i}{u_i} \sum_{j=1}^{i} u_j \eta_{j,i}, \tag{2.12}$$

We call this method one order moment conserving method (OOM).

Proposition 2.1. *The proposed numerical scheme* (2.11) *holds the mass conservation law if* $\hat{S}_i = \frac{S_i}{u_j} \sum_{i=1}^{j} u_i \eta_{i,j}$.

Proof. Take a summation $\sum_{i=1}^{I}$ on both sides the equation (2.11), we have

$$\frac{\mathrm{d}\sum_{i=1}^{I} \hat{m}_i}{\mathrm{d}t} = \sum_{i=1}^{I} \sum_{j=i}^{I} S_j \frac{u_i}{u_j} \hat{m}_j \eta_{i,j} - \sum_{i=1}^{I} \hat{S}_i \hat{m}_i. \tag{2.13}$$

Replace the index i to k in the second term of the RHS, we get

$$\frac{\mathrm{d}\sum_{i=1}^{I} \hat{m}_i}{\mathrm{d}t} = \sum_{i=1}^{I} \sum_{j=i}^{I} S_j \frac{u_i}{u_j} \hat{m}_j \eta_{i,j} - \sum_{j=1}^{I} \hat{S}_j \hat{m}_j. \tag{2.14}$$

Now change the order of the first summation, leads to

$$\frac{\mathrm{d}\sum_{i=1}^{I}\hat{m}_i}{\mathrm{d}t}=\sum_{j=1}^{I}\hat{m}_j\left(\sum_{i=1}^{j}S_j\frac{u_i}{u_j}\eta_{i,j}-\hat{S}_j\right). \tag{2.15}$$

By introducing the value of $\hat{S}_j$ from equation (2.12), it gives

$$\frac{\mathrm{d}\sum_{i=1}^{I}\hat{m}_i}{\mathrm{d}t}=\sum_{j=1}^{I}S_j\hat{m}_j\left(\sum_{i=1}^{j}Sj\frac{u_i}{u_j}\eta_{i,j}-\sum_{i=1}^{j}S_j\frac{u_i}{u_j}\eta_{i,j}\right). \tag{2.16}$$

Hence

$$\frac{\mathrm{d}\sum_{i=1}^{I}\hat{m}_i}{\mathrm{d}t}=0,$$

which implies that the first order moment is conserved, that is, the formulation (2.11) holds the mass conservation property. Here, OOM refers to a finite volume scheme which conserves one order moment. □

2.2. Number consistent and mass conserving scheme (TOM)

It is important to note that the OOM finite volume scheme merely focuses on conserving the total mass in the system, however, do not give any account for the accurate prediction of the zeroth order moment. But it will be interesting to observe that to what extend this scheme predicts the zeroth order moment accurately. The zeroth order moment plays a very significant role in predicting the average size of the particles $\bar{u}=\frac{\mu_1}{\mu_0}$ in the particulate processes such as crystallization, deploymerization and granulation [20, 32, 38]. This implies the accurate prediction of the zeroth order moment is very crucial and leads to the higher accuracy of the average size of particles in the system. Therefore, next our aim will be to develop a finite volume scheme whose features include the accurate prediction of both zeroth and first order moments. In addition, it will be interested to observe that to what extent this scheme captures the second order moment accurately which is significant to calculate the total area of the particles. We named this approach two order moments (TOM) conserving finite volume scheme.

To achieve this two order moment conserving method, the selection functions in the first and second term of equation (2.7) are modified as follows:

$$\frac{\mathrm{d}\hat{m}_i}{\mathrm{d}t}=\sum_{j=i}^{I}S_j^b\hat{m}_j\frac{u_i}{u_j}\eta_{i,j}-S_i^a\hat{m}_i. \tag{2.17}$$

Here

$$S_j^b=\frac{S_ju_j(v(u_j)-1)}{\sum_{i=1}^{j-1}(u_j-u_i)\eta_{i,j}}, \tag{2.18}$$

and

$$S_j^d=\frac{S_j^b}{u_j}\sum_{i=1}^{j}u_i\eta_{j,i},\qquad i=2,3,\ldots,I, \tag{2.19}$$

where $v(u_j)$ denotes the number of particles formed from the fragmentation of particle property u_j and the values of S_1^b and S_1^d are considered to be zero. Let us now prove the mass conservation law and preservation

of zeroth order moment for the finite volume scheme (2.17). The numerical scheme is consistent with number preservation property if it satisfies the follows relation:

$$\frac{\mathrm{d}}{\mathrm{d}t}\sum_{j=1}^{I}\frac{\hat{N}_j}{u_j} = \sum_{j=1}^{I} S_j \frac{\hat{m}_j}{u_j}(v(u_j)-1). \tag{2.20}$$

where $\hat{N}_j = \frac{\hat{m}_j}{u_j}$.

Proposition 2.2. *The proposed numerical scheme (2.17) holds the mass conservation law, that is, no mass leave the system if* $S_j^b = \frac{S_j u_j (v(u_j)-1)}{\sum_{i=1}^{j-1}(u_j-u_i)\eta_{i,j}}$ *and* $S_i^d = \frac{S_i^b}{u_i}\sum_{j=1}^{i} u_j\eta_{i,j}$.

Proof. Take a summation $\sum_{i=1}^{I}$ on both sides the equation (2.17), we have

$$\frac{\mathrm{d}\hat{m}_i}{\mathrm{d}t} = \sum_{i=1}^{I}\sum_{j=i}^{I} S_j^b \hat{m}_j \frac{u_i}{u_j}\eta_{i,j} - \sum_{i=1}^{I} S_i^d \hat{m}_i. \tag{2.21}$$

Change the order of summation in the first term, interchange the index i to j in the second terms and substituting the values of S_j^b and S_i^d, the above expression becomes

$$\frac{\mathrm{d}\sum_{i=1}^{I}\hat{m}_i}{\mathrm{d}t} = \sum_{j=1}^{I}\frac{\hat{m}_j S_j u_j (v(u_j)-1)}{\sum_{i=1}^{j-1}(u_j-u_i)\eta_{i,j}}\sum_{i=1}^{j}\frac{u_i}{u_j}\eta_{i,j} - \sum_{j=1}^{I}\frac{\hat{m}_j S_j u_j (v(u_j)-1)}{u_i\sum_{i=1}^{j-1}(u_j-u_i)\eta_{i,j}}\sum_{i=1}^{j} u_j\eta_{i,j}. \tag{2.22}$$

After simplification, we get

$$\begin{aligned}\frac{\mathrm{d}\sum_{i=1}^{I}\hat{m}_i}{\mathrm{d}t} &= \sum_{j=1}^{I}\frac{\hat{m}_i S_j u_j (v(u_j)-1)}{\sum_{i=1}^{j-1}(u_j-u_i)\eta_{i,j}}\left(\sum_{i=1}^{j} u_j\eta_{i,j} - \sum_{i=1}^{j} u_j\eta_{i,j}\right),\\ &= 0.\end{aligned}$$

This further implies

$$\hat{m}_i = \text{constant}. \tag{2.23}$$

Hence the total mass in the system remains constant with the evolution of time, that is, the mass conservation property holds for the formulation (2.17). □

Proposition 2.3. *The proposed numerical scheme (2.17) is consistent with the zeroth order moment if* $S_j^b = \frac{S_j u_j (v(u_j)-1)}{\sum_{i=1}^{j-1}(u_j-u_i)\eta_{i,j}}$ *and* $S_i^d = \frac{S_i^b}{u_i}\sum_{j=1}^{i} u_j\eta_{i,j}$.

Proof. Divide both side of equation (2.17) by u_i and take a summation $\sum_{i=1}^{I}$ gives

$$\frac{\mathrm{d}\hat{m}_i}{\mathrm{d}t} = \sum_{i=1}^{I}\frac{1}{u_i}\sum_{j=i}^{I} S_j^b \hat{m}_j \frac{u_i}{u_j}\eta_{i,j} - \sum_{i=1}^{I}\frac{1}{u_i} S_i^d \hat{m}_i. \tag{2.24}$$

Change the order of summation and substituting the values of S_j^b and S_i^d leads to

$$\frac{\mathrm{d}\sum_{i=1}^{I}\hat{N}_i}{\mathrm{d}t} = \sum_{j=1}^{I}\frac{\hat{m}_j}{u_j}\frac{S_j u_j(v(u_j)-1)}{\sum_{i=1}^{j}(u_j-u_i)\eta_{i,j}}\sum_{i=1}^{j}\eta_{i,j} - \sum_{j=1}^{I}\frac{1}{u_j}\frac{S_j u_j(v(u_j)-1)}{\sum_{j=1}^{i-1}(u_j-u_i)\eta_{i,j}}\sum_{i=1}^{j}u_i\eta_{i,j}\hat{m}_i. \tag{2.25}$$

After simplification, we get

$$\begin{aligned}\frac{\mathrm{d}\sum_{i=1}^{I}\hat{N}_i}{\mathrm{d}t} &= \sum_{j=1}^{I}\frac{\hat{m}_j}{u_j}\frac{S_j u_j(v(u_j)-1)}{\sum_{j=1}^{i}(u_j-u_i)\eta_{i,j}}\left(\sum_{i=1}^{j}\eta_{i,j} - \sum_{i=1}^{j}\frac{u_i}{u_j}\eta_{i,j}\right)\\ &= \sum_{i=1}^{I}\frac{\hat{m}_j}{u_j}\frac{S_j u_j(v(u_j)-1)}{\sum_{i=1}^{j}(u_j-u_i)\eta_{i,j}}\frac{1}{u_i}\left(\sum_{i=1}^{j}u_j\eta_{i,j} - \sum_{i=1}^{j}u_i\eta_{i,j}\right)\\ &= \sum_{j=1}^{I}\frac{\hat{m}_j}{u_j}\frac{S_j(v(u_j)-1)}{\sum_{i=1}^{j}(u_j-u_i)\eta_{i,j}}\left(\sum_{i=1}^{j}(u_i-u_j)\eta_{i,j}\right)\\ &= \sum_{j=1}^{I}S_j\frac{\hat{m}_j}{u_j}(v(u_j)-1).\end{aligned} \tag{2.26}$$

The above expression is same as the relation provided in equation (2.20). Therefore, the formulation (2.17) shows consistency with the zeroth order moment. □

3. Convergence analysis

The convergence analysis of the both finite volume schemes are carrying out by writing the equations in vector form. Suppose that vectors $\mathbf{m}$ and $\hat{\mathbf{m}}$ represent the exact average and numerical values, respectively. The vector form of the discrete equations (2.11) and (2.17) can be written as

$$\frac{\partial\hat{\mathbf{m}}}{\partial t} = J(\hat{g}), \quad \hat{\mathbf{m}}(0) = \mathbf{m}(0). \tag{3.1}$$

Here, $J \in \mathcal{R}^I$ are the functions of $\hat{m}$ with the components of one order moment conserving methods are

$$\hat{B}_i^{\,\mathrm{OOM}}(\hat{\mathbf{m}}) = \sum_{j=i}^{I}S_j\hat{m}_j\frac{u_i}{u_j}\eta_{i,j}, \tag{3.2}$$

and

$$\hat{D}_i^{\,\mathrm{OOM}}(\hat{\mathbf{m}}) = \hat{S}_i\hat{m}_i, \tag{3.3}$$

and the components of two order moment conserving methods are

$$\hat{B}_i^{\,\mathrm{TOM}}(\hat{\mathbf{m}}) = \sum_{j=i}^{I}\hat{S}_j^b\hat{m}_j\frac{u_i}{u_j}\eta_{i,j}, \tag{3.4}$$

and

$$\hat{D}_i^{\,\mathrm{TOM}}(\hat{\mathbf{m}}) = \hat{S}_i^d\hat{m}_i. \tag{3.5}$$

Therefore, the final form of equation is

$$J_i(\hat{\mathbf{m}}) = \hat{B}_i(\hat{m}) - \hat{D}_i(\hat{m}). \tag{3.6}$$

The convergence of the discrete system will be conducted with the help of theorem provided in the further section. Firstly, the define the norm L^1 considered for convergence as

$$\|\mathbf{m}(t)\| = \sum_{i=1}^{I} |m_i(t)| \Delta u_i. \tag{3.7}$$

Some important definitions required for discussing the convergence analysis of the numerical schemes are provided in A. Following from the Theorem A.3, if the equations (2.11) and (2.17) follow the Lipschitz Condition and shows consistency. Then using the Theorem A.4, the convergence of both finite volume schemes can be obtained.

3.1. Lipschitz condition for OOM FVS

Let us assume that the kernels S and b are twice continuously differentiable functions over $[0, u_{\max}]$ and $[0, u_{\max}] \times [0, u_{\max}]$, respectively, then there exist a constant

$$C = \max_{u \in (0, u_{\max}]} S_i v(u_i) < \infty,$$

such that the Lipschitz condition on J is satisfied for all $\mathbf{m}$ and $\hat{\mathbf{m}} \in \mathbb{R}^I$, that is,

$$\|\mathbf{J}(\mathbf{m}) - \mathbf{J}(\hat{\mathbf{m}})\| \leq L \|\mathbf{m} - \hat{\mathbf{m}}\|.$$

Let us consider

$$\|\mathbf{J}(\mathbf{m}) - \mathbf{J}(\hat{\mathbf{m}})\| = \sum_{i=1}^{I} \left| \sum_{j=i}^{I} S_j \frac{u_i}{u_j} \eta_{i,j} (m_j - \hat{m}_j) - \hat{S}_i (m_i - \hat{m}_i) \right|,$$

Since the daughter particle (u_i) is always smaller than the mother particle (u_j), that is, $u_i \leq u_j$ for all $i = 1, 2, 3, \ldots, j$ implies

$$\|\mathbf{J}(\mathbf{m}) - \mathbf{J}(\hat{\mathbf{m}})\| \leq \sum_{i=1}^{I} \sum_{j=i}^{I} S_j \eta_{i,j} \frac{u_j}{u_j} |m_j - \hat{m}_j| + \sum_{i=1}^{I} \hat{S}_i |m_i - \hat{m}_i|. \tag{3.8}$$

Changing the order in the first summation and substitute the value of $\hat{S}_i$, we have

$$\|\mathbf{J}(\mathbf{m}) - \mathbf{J}(\hat{\mathbf{m}})\| \leq \sum_{j=1}^{I} S_j |m_j - \hat{m}_j| \sum_{i=1}^{j} \eta_{i,j} + \sum_{i=1}^{I} \frac{S_i}{u_j} \sum_{i=1}^{j} u_i \eta_{i,j} |m_i - \hat{m}_i|. \tag{3.9}$$

Using again $u_i \leq u_j$, we have $\hat{S}_i = \frac{S_j}{u_j} \sum_{i=1}^{j} u_i \eta_{i,j} \leq \frac{S_j}{u_j} \sum_{i=1}^{j} u_j \eta_{i,j} = S_j v(u_i)$ and replacing this value in above equation leads to

$$\|\mathbf{J}(\mathbf{m}) - \mathbf{J}(\hat{\mathbf{m}})\| \leq \sum_{i=1}^{I} S_i v(u_i) |m_i - \hat{m}_i| + \sum_{i=1}^{I} S_i v(u_i) |m_i - \hat{m}_i|. \tag{3.10}$$

This further implies

$$\begin{aligned}\|\mathbf{J}(\mathbf{m}) - \mathbf{J}(\hat{\mathbf{m}})\| &\leq 2\sum_{i=1}^{I} S_i v(u_i)\,|m_i - \hat{m}_i| \\ &= 2\sum_{i=1}^{I}\left(\max_i S_i v(u_i)\right)|m_i - \hat{m}_i| \\ &= 2\max_{u\in(0,u_{\max}]} S(u)v(u)\|\mathbf{m} - \hat{\mathbf{m}}\| \\ &\leq C\|\mathbf{m} - \hat{\mathbf{m}}\|. \end{aligned} \tag{3.11}$$

Here $C = 2\max_{u\in(0,u_{\max}]} S(u)v(u) < \infty$ and the Lipschitz constant does not dependent on Δu. Hence, it proves the Lipschitz condition on $\mathbf{J}$. Let us now proceed to discuss that the formulation (2.11) shows consistency or not.

3.2. Consistency of the OOM FVS

Theorem 3.1. *Suppose that the selection function S and breakage kernel b are twice continuously differentiable functions over $(0, u_{\max}]$ and $(0, u_{\max}] \times (0, u_{\max}]$, respectively. Then, the numerical solution of the formulation (2.11) is non-negative and consistent, with a truncation error of order 2, independently of the type of grid consider for continuous domain discretization. Moreover, the scheme is convergent and the order of convergence is the same as the order of consistency.*

Proof. For establishing the above theorem, the necessary property which numerical scheme has to follow is the nonnegativity, consistency, and convergence. The nonnegativity of the numerical scheme is given below:

Nonnegativity. Since the mass of system cannot negative, therefore for any nonnegative mass distribution $\hat{m} \in \mathbb{R}^I$, (for all $\hat{m} \geq 0$ which has *ith* component equals to zero). So, equations (3.2) and (3.3) gives

$$\hat{B}_i^{\,\mathrm{OOM}}(\hat{\mathbf{m}}) \geq 0 \quad \text{and} \quad \hat{D}_i^{\,\mathrm{OOM}}(\hat{\mathbf{m}}) = 0.$$

The equation (3.6) implies $J_i(\hat{\mathbf{m}}) = \hat{B}_i^{\,\mathrm{OOM}}(\hat{\mathbf{m}}) - \hat{D}_i^{\,\mathrm{OOM}}(\hat{\mathbf{m}}) \geq 0$. Moreover, for any $i = 1, 2, \ldots, I$, Theorem A.3 and Proposition A.4 imply the nonnegativity of the solution.

Consistency. The ith component of the spatial truncation error (From Def. A.1) is

$$\sigma_i(t) = \frac{\mathrm{d}m_i(t)}{\mathrm{d}t} - J_i(m_i(t)).$$

Using (2.4), (2.5), (3.2)and (3.3), the above equation becomes

$$\sigma_i(t) = B_i - \hat{B}_i^{\,\mathrm{OOM}} - \left(D_i - \hat{D}_i^{\,\mathrm{OOM}}\right). \tag{3.12}$$

Substituting the values from equations (2.4) and (3.2), the $B_i - \hat{B}_i^{\,\mathrm{OOM}}$ can be simplified as follows:

$$B_i - \hat{B}_i^{\,\mathrm{OOM}} = \sum_{j=i}^{I} S_j m_j \eta_{i,j} - \sum_{j=i}^{I} S_j m_j \eta_{i,j} + \mathcal{O}(\Delta u^2). \tag{3.13}$$

This implies that $B_i - \hat{B}_i^{\,\mathrm{OOM}} = \mathcal{O}(\Delta u^2)$.

Use the values from equations (2.5) and (3.3), now let us discuss the order of consistency of $D_i - \hat{D}_i^{\,\mathrm{OOM}}$ term similar to birth term given as below

$$D_i - \hat{D}_i^{\,\mathrm{OOM}} = (S_i - \hat{S}_i)m_i + \mathcal{O}(\Delta u^2). \tag{3.14}$$

Replacing the value of $\hat{S}_i$ in the above equation, we get

$$D_i - \hat{D}_i^{\text{OOM}} = \left(1 - \frac{1}{u_j}\sum_{i=1}^{j} u_i\eta_{i,j}\right) S_i m_i + \mathcal{O}(\Delta u^2),$$
$$= \frac{1}{u_j}\left(u_j - \sum_{i=1}^{j} u_i\eta_{i,j}\right) S_i m_i + \mathcal{O}(\Delta u^2). \tag{3.15}$$

Using $u_j = \int_0^{u_j} ub(u,u_j)\mathrm{d}u$, we have

$$D_i - \hat{D}_i^{\text{OOM}} = \frac{1}{u_j}\left(\int_0^{u_j} ub(u,u_j)\mathrm{d}u - \sum_{i=1}^{j} u_i\eta_{i,j}\right) S_i m_i + \mathcal{O}(\Delta u^2)$$
$$= \frac{1}{u_j}\left(\sum_{j=1}^{i}\int_{u_{j-1/2}}^{\phi_i^j} (u-u_j)b(u,u_i)\mathrm{d}u\right)$$
$$= \frac{1}{u_j}\left(\int_{u_{j-1/2}}^{u_{j+1/2}} (u-u_j)b(u,u_i)\mathrm{d}u + \int_{u_{i-1/2}}^{u_i} (u-u_i)b(u,u_i)\mathrm{d}u\right). \tag{3.16}$$

Further implement the MDA to first summation for $j = 1, 2, 3, \ldots, i-1$ and right end approximation (REP) for $j = i$ in the above equation gives second order accuracy for the numerator of above equation.

Hence we have

$$D_i - \hat{D}_i^{\text{OOM}} = \mathcal{O}(\Delta u^2). \tag{3.17}$$

Replacing the values from equations (3.13) and (3.17) in equation (3.12), we get

$$\sigma_i(t) = \mathcal{O}(\Delta u^2). \tag{3.18}$$

This further gives

$$||\sigma(t)|| = \mathcal{O}(\Delta u^2), \tag{3.19}$$

which do not show any dependency on any grid or step size.

Convergence. It is demonstrated that the numerical solution satisfies the Lipschitz condition and also shows second order consistency. Using these results and Theorem A.4 imply that the order of convergence for the numerical scheme is same as the order of consistency, that is, the numerical scheme exhibits second order accuracy. □

3.3. Lipschitz condition for TOM FVS

Let us consider

$$\|\mathbf{J}(\mathbf{m}) - \mathbf{J}(\hat{\mathbf{m}})\| = \sum_{i=1}^{I}\left|\sum_{j=i}^{I} \hat{S}_j^b \frac{u_i}{u_j}\eta_{i,j}(m_j - \hat{m}_j) - \hat{S}_j^d(m_i - \hat{m}_i)\right|.$$

The above equation further simplifies to

$$\|\mathbf{J}(\mathbf{m}) - \mathbf{J}(\hat{\mathbf{m}})\| \le \overbrace{\sum_{i=1}^{I}\sum_{j=i}^{I} \hat{S}_j^b \frac{u_i}{u_j}\eta_{i,j}\,|m_j - \hat{m}_j|}^{M_1} + \overbrace{\sum_{i=1}^{I} \hat{S}_j^d\,|m_i - \hat{m}_i|}^{M_2}.$$

Let us now solve the summations M_1 and M_2 separately.

Simplification of M_1 term. To simplify the term M_1, first change the order of the summation, we get

$$M_1 = \sum_{i=1}^{I}\sum_{j=1}^{i} \hat{S}_j^b \frac{u_i}{u_j}\eta_{i,j}\left|m_j - \hat{m}_j\right|. \tag{3.20}$$

Using $u_i \le u_j$ and substituting the value of $\hat{S}_j^b$ with $\hat{S}_1^b = 0$ in the above equation, it gives

$$\begin{aligned} M_1 \le& \sum_{j=2}^{I}\sum_{i=1}^{j} S_j\eta_{i,j}|m_k - \hat{m}_k|\left[\frac{u_j v(u_j)}{\sum_{i=1}^{j}(u_j-u_i)\eta_{i,j}} - \frac{u_j}{\sum_{i=1}^{j}(u_j-u_i)\eta_{i,j}}\right] \\ =& \sum_{j=2}^{I}\sum_{i=1}^{j} S_j\eta_{i,j}|m_j - \hat{m}_j|\left[\frac{(u_j-u_i)v(u_j)}{\sum_{i=1}^{j}(u_j-u_i)\eta_{i,j}} - \frac{u_j v(u_j)}{\sum_{i=1}^{j}(u_j-u_i)\eta_{i,j}}\right] - \sum_{j=2}^{I}\sum_{i=1}^{j}\frac{S_j\eta_{i,j}|m_j-\hat{m}_j|u_j}{\sum_{i=1}^{j}(u_j-u_i)\eta_{i,j}}. \end{aligned} \tag{3.21}$$

Simplification and rearranging gives the following equation

$$M_1 \le \sum_{j=2}^{I} v(u_j)S_j|m_j-\hat{m}_j| + \sum_{j=2}^{I}\frac{v(u_j)S_j\eta_{i,j}|m_j-\hat{m}_j|}{\sum_{i=1}^{j}(u_j-u_i)\eta_{i,j}}\left[\sum_{i=1}^{j}u_i\eta_{i,j} - u_j\right]. \tag{3.22}$$

Since $b(u,u_j)$ is twice continuously differentiable function and further using the midpoint and the right end approximation of the integrals, we obtain

$$u_j = \int_0^{u_j} ub(u,u_j)\mathrm{d}u = \sum_{i=1}^{j}\int_{u_{j-1/2}}^{\phi_j^i} ub(u,u_j)\mathrm{d}u = \sum_{i=1}^{j} u_i\eta_{i,j} + \mathcal{O}(\Delta u)^2.$$

This further gives

$$\left|u_i - \sum_{i=1}^{j} u_i\eta_{i,j}\right| = \mathcal{O}(\Delta u)^2 \le C_1(\Delta u)^2, \text{ where } C_1 < \infty \text{ is a constant.} \tag{3.23}$$

Additionally, for $j = 2,3,\ldots,I$, we have

$$\sum_{i=1}^{j}(u_j-u_i)\eta_{i,j} \ge (u_j-u_{i-1})\sum_{i=1}^{j-1}\eta_{i,j} \ge \Delta u_j\int_0^{u_{j-1/2}} b(u,u_j)\mathrm{d}u \ge C_2(\delta u), \tag{3.24}$$

where C_2 is a constant, satisfying

$$0 < C_2 = \min_{j\in\{2,3,\ldots,I\}}\left[\int_0^{u_{j-1/2}} b(u,u_j)\mathrm{d}u\right]. \tag{3.25}$$

Using equation (2.1) and above relations in equation (3.22), we reaches to

$$\begin{aligned} M_1 \le& \sum_{j=2}^{I} v(u_j)S_j|m_j-\hat{m}_j| + \sum_{j=2}^{I}\frac{(\Delta u)^2}{\delta u}\frac{C_1}{C_2}v(u_j)S_j|m_j-\hat{m}_j| \\ \le& \left[1+\frac{C_1}{C_2}Hu_{\max}\right]\sum_{j=1}^{I} v(u_j)S_j|m_j-\hat{m}_j|\Delta u_j \qquad (3.26) \\ \le& \left[1+\frac{C_1}{C_2}Hu_{\max}\right]\max_{j\in\{2,3,\ldots,I\}}[v(u)S(u)]\sum_{j=1}^{I}|m_j-\hat{m}_j| \qquad (3.27) \end{aligned}$$

Here $\delta u = \min_i \Delta u_i$. The above relation can further be simplified to

$$M_1 \leq C_3 ||\mathbf{m} - \hat{\mathbf{m}}||. \tag{3.28}$$

where

$$M_3 = Q \max_{u \in \{2,3,\ldots,u_{\max}\}} [v(u)S(u)] \leq \infty$$

and $Q = [1 + \frac{C_1}{C_2} H u_{\max}]$.

Simplification of M_2 term. Let us further simplify the second term M_2 given in equation (3.8)

$$M_2 = \sum_{j=1}^{I} |m_j - \hat{m}_j| S_j^d = \sum_{j=1}^{I} |m_j - \hat{m}_j| \frac{S_j^b}{u_j} \sum_{i=1}^{j} u_i \eta_{i,j}.$$

Using the fact that $u_i \leq u_j \ \forall \ i = 1, 2, 3, \ldots, j$,

$$M_2 \leq \sum_{i=1}^{I} |m_j - \hat{m}_j| \frac{S_j^b}{u_j} \sum_{j=1}^{i} u_i \eta_{i,j}.$$

Now change the order of the integration, we have

$$M_2 \leq \sum_{i=1}^{I} \sum_{j=i}^{I} |m_j - \hat{m}_j| \frac{S_j^b}{u_j} u_i \eta_{i,j} = M_1.$$

This gives

$$M_2 \leq C_3 ||\mathbf{m} - \hat{\mathbf{m}}||. \tag{3.29}$$

Using the equations (3.28) and (3.29), the equation (3.8) takes the following form:

$$\|\mathbf{J}(\mathbf{m}) - \mathbf{J}(\hat{\mathbf{m}})\| \leq M ||\mathbf{m} - \hat{\mathbf{m}}||, \tag{3.30}$$

where $M = 2C_3 < \infty$ is a Lipschitz constant.

3.4. Consistency of the TOM FVS

Similar to the OOM, the consistency of the TOM is discussed using the Theorem 3.1 to derive the order of convergence of the scheme.

Nonnegativity. Since the total mass in the system is always positive, therefore for any non-negative mass distribution $\hat{m} \in \mathbb{R}^I$, (for all $\hat{m} \geq 0$ which has *ith* component equals to zero). So, equations (3.4) and (3.5) gives

$$\hat{B}_i^{\text{TOM}}(\hat{\mathbf{m}}) \geq 0 \quad \text{and} \quad \hat{D}_i^{\text{TOM}}(\hat{\mathbf{m}}) = 0.$$

The equation (3.6) implies $J_i(\hat{\mathbf{m}}) = \hat{B}_i^{\text{TOM}}(\hat{\mathbf{m}}) - \hat{D}_i^{\text{TOM}}(\hat{\mathbf{m}}) \geq 0$. Moreover, for any $i = 1, 2, \ldots, I$, Theorem A.3 and Proposition A.4 imply the nonnegativity of the solution.

Consistency. Using the Definition A.1, the jth component of the spatial truncation error can be written as

$$\sigma_i(t) = \frac{\mathrm{d}m_i(t)}{\mathrm{d}t} - J_i(m_i(t)).$$

Using (2.4), (2.5), (3.4)and (3.5), the above equation becomes

$$\sigma_i(t) = \overbrace{B_i - \hat{B}_i^{\text{TOM}}}^{P_1} - \overbrace{\left(D_i - \hat{D}_i^{\text{TOM}}\right)}^{P_2}. \tag{3.31}$$

Simplification of P_1 term. Now consider the first term P_1 of the equation (3.31),

$$P_1 = B_j - \widehat{B}_j = \left[\sum_{j=i}^{I} \frac{u_i}{u_j} S_j m_j \eta_{i,j} - \sum_{j=i}^{I} u_j \eta_{i,j} \frac{u_i}{u_j} S_j^b\right] + \mathcal{O}(\Delta u^2). \tag{3.32}$$

Combining the terms, we get

$$\begin{aligned} P_1 &= \sum_{j=i}^{I} m_j \eta_{i,j} \frac{u_i}{u_j} \left(S_j - S_j^b\right) + \mathcal{O}(\Delta u^2) \\ &= \left[\sum_{j=i}^{I} S_j m_j \eta_{i,j} \frac{u_i}{u_j} \left(1 - \frac{u_j(v(u_j) - 1)}{\sum_{i=1}^{j-1}(u_j - u_i)\eta_{i,j}}\right)\right] + \mathcal{O}(\Delta u^2) \\ &= \left[\sum_{j=i}^{I} S_j m_j \eta_{i,j} \frac{u_i}{u_j} \left(\frac{u_j - \sum_{i=1}^{j} u_j \eta_{i,j}}{\sum_{i=1}^{j-1}(u_j - u_i)\eta_{i,j}}\right)\right] + \mathcal{O}(\Delta u^2). \end{aligned} \tag{3.33}$$

Using the application of midpoint and right end quadrature approximations, the numerator of above equation can be shown of the order 2 whereas the denominator is of order 0. This gives

$$P_1 = \mathcal{O}(\Delta y^2). \tag{3.34}$$

Simplification of P_2 term. Let us now obtain the order of consistency for the P_2 term of equation (3.12)

$$P_2 = (S_j - S_j^d)m_j + \mathcal{O}(\Delta u^2). \tag{3.35}$$

Replace the value of S_j^d from equation (2.19) in above equation, we get

$$D_j - \widehat{D}_j = \left(S_j - \frac{S_j^b}{u_j} \sum_{i=1}^{j} u_j \eta_{i,j}\right) m_j + \mathcal{O}(\Delta u^2), \tag{3.36}$$

$$= \frac{1}{u_j} \left(u_j - S_j^b \sum_{i=1}^{j} u_j \eta_{i,j}\right) S_j m_j + \mathcal{O}(\Delta u^2). \tag{3.37}$$

It can be noted that

$$u_j = \int_0^{u_j} ub(u, u_j)\mathrm{d}u = \sum_{j=1}^{i} \int_{u_{j-1/2}}^{p_j^i} ub(u, u_k)\mathrm{d}u = \sum_{i=1}^{j} u_j \eta_{i,j} + \mathcal{O}(\Delta u^2).$$

Using u_j from the above equation in (3.36) leads to

$$P_2 = \left(S_j - \frac{S_j u_j (v(u_j) - 1)}{\sum_{i=1}^{j-1}(u_j - u_i)\eta_{i,j}}\right) \left(\frac{1}{u_j} \sum_{i=1}^{j} \eta_{i,j}\right) m_j + \mathcal{O}(\Delta u^2). \tag{3.38}$$

As proved earlier that $1 - \frac{u_j(v(u_j)-1)}{\sum_{i=1}^{j-1}(u_j - u_i)\eta_{i,j}} = \mathcal{O}(\Delta u^2)$, we have

$$P_2 = \mathcal{O}(\Delta u^2). \tag{3.39}$$

Hence, from equation (3.31) using equations (3.34) and (3.39), we get

$$\sigma_j(t) = \mathcal{O}(\Delta u^2) \Rightarrow \|\sigma(t)\| = \mathcal{O}(\Delta u^2).$$

Convergence. From Theorem A.4 and the above results on consistency prove that the TOM also converges to the second order same as the order of convergence of OOM.

4. Numerical testing and discussion

The accuracy and efficiency of the numerical methods is tested by comparing the numerical results with analytical solutions for various combination of selection functions and breakage kernels.For the testing two initial conditions (ICs) are considered (a) monodisperse ($m(0,u) = \delta(u-1)$), and (b) exponential ($m(0,u) = \exp(-u)$) initial conditions. Following combinations of ICs, selection functions and breakage kernels are used to compare the results:

Case 1. Binary breakage kernel and linear selection function with monodisperse IC.
Case 2. Binary breakage kernel and linear selection function with exponential IC.
Case 3. Binary breakage kernel and constant selection function with monodisperse IC.
Case 4. Binary breakage kernel and constant selection function with exponential IC.

The theoretical (analytical) solutions for the number density functions and integral moments corresponding to the Cases 1 and 2 can be found in Ziff [48]. However, for the Cases 3 and 4, no theoretical solutions for the number density functions are available in the literature, however, the numerical results are compared against the theoretical results in terms of integral moments and average size particles. In order to observe the errors in each cell of the computational domain, the weighted sectional error in the number density functions are also estimated using the following relation:

$$\lambda_i(t) = \frac{\sum_{j=1}^{I} |n_j^{\text{exc}} - n_j^{\text{num}}| \Delta u_j^i u_j^i}{\sum_{j=1}^{I} n_j^{\text{exc}} \Delta u_j^i u_j^i}, \tag{4.1}$$

where $\lambda_i(t)$ for $i = 0$ and $\lambda_i(t)$ for $i = 1$ compute the relative weighted sectional errors in zeroth and first order moments, respectively.

4.1. Test Case 1

we began the exercise of comparison by taking into consideration the binary breakage kernel ($b(u,v) = \frac{2}{v}$) and linear selection function ($S(u) = u$) with monodisperse IC. The computational domain [10^{-9} 1] is discretized into 30 nonuniform cells and the simulations are run from time 0 to 100.

Figure 4 demonstrates the comparison of numerical results against the theoretical results. The zeroth order moment is approximated well by TOM FVS, however, the OOM FVS shows underpredicton from the theoretical result (refer to Fig. 4a). Furthermore, both methods conserved the total mass in the system as expected. The second order moment which signifies the total area of the particles is more accurately predicted by the TOM FVS than the OOM FVS as it shows more deviation from the theoretical result. It can be noticed that no specific measure has been taken for the accuracy of the second order moment, still the TOM FVS tends to produce this result with higher precision.

In addition, the plots of number of particles in each cell and the number density function *versus* the representative of cell are calculated with higher accuracy by the TOM FVS than OOM FVS as shown in Figures 4b and 4c. The average size of particles which signifies the ratio of the first order moment to the zeroth order moment is also plotted in Figure 4d. The TOM shows higher precision than the OOM in calculating the average size particles obtained in the system due to the fragmentation process. In order to observe the deviation of numerical results from the theoretical result in each cell, the sectional errors in the number density function are estimated

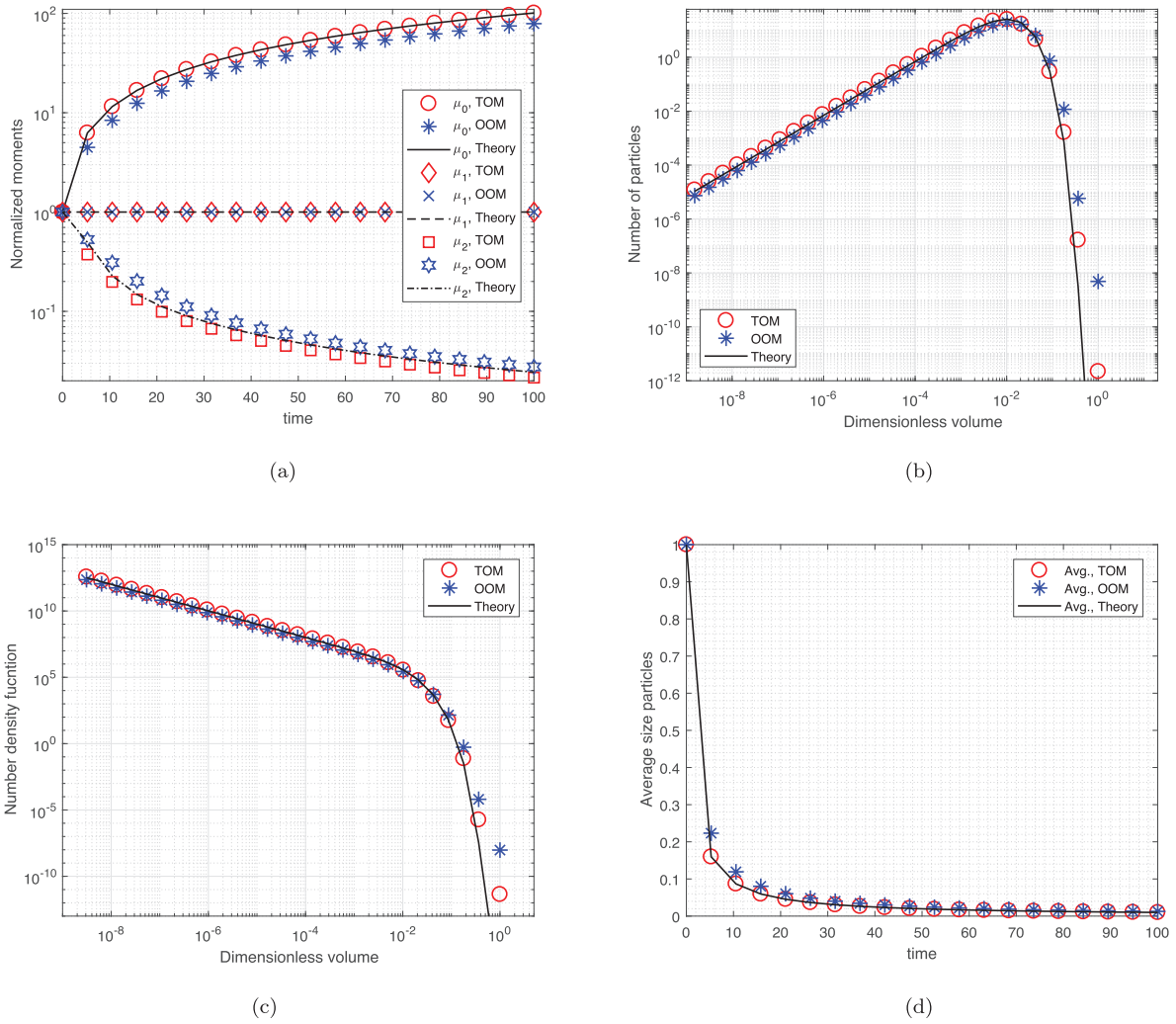

FIGURE 4. Comparison of normalized moments, number of particles, number density function and average particle size using Case 1. (a) Normalized moments. (b) Number of particles. (c) Number density function. (d) Average size particles.

using the expression (4.1) are listed in Table 1. Table reveals that the TOM FVS predicted the results with more accuracy than the OOM FVS. Furthermore, the sectional errors reduce to 70% once a grid consists of 60 nonunifrom cells is used to solve the reduced fragmentation model. However, still the TOM FVS performs much better than the OOM FVS.

4.2. Test Case 2

Now the testing of the numerical methods is conducted using the linear selection function and binary breakage kernel for a exponential initial condition. The computational domain $[10^{-7}\ 10]$ is divided into 30 nonuniform cells and the simulations are run till time $t = 10$.

Analogous to previous case, the zeroth, first and second order moments are well predicted by the TOM FVS for the Case 2 whereas the OOM FVS deviates significantly from the theoretical results as depicted in

TABLE 1. Weighted sectional errors in the number density function for Test Case 1.

λ	OOM 30 cells	TOM 30 cells	OOM 60 cells	TOM 60 cells
λ_0	0.23110	0.07290	0.06545	0.01854
λ_1	0.21010	0.09234	0.05581	0.02430
λ_2	0.28413	0.11698	0.07008	0.03200

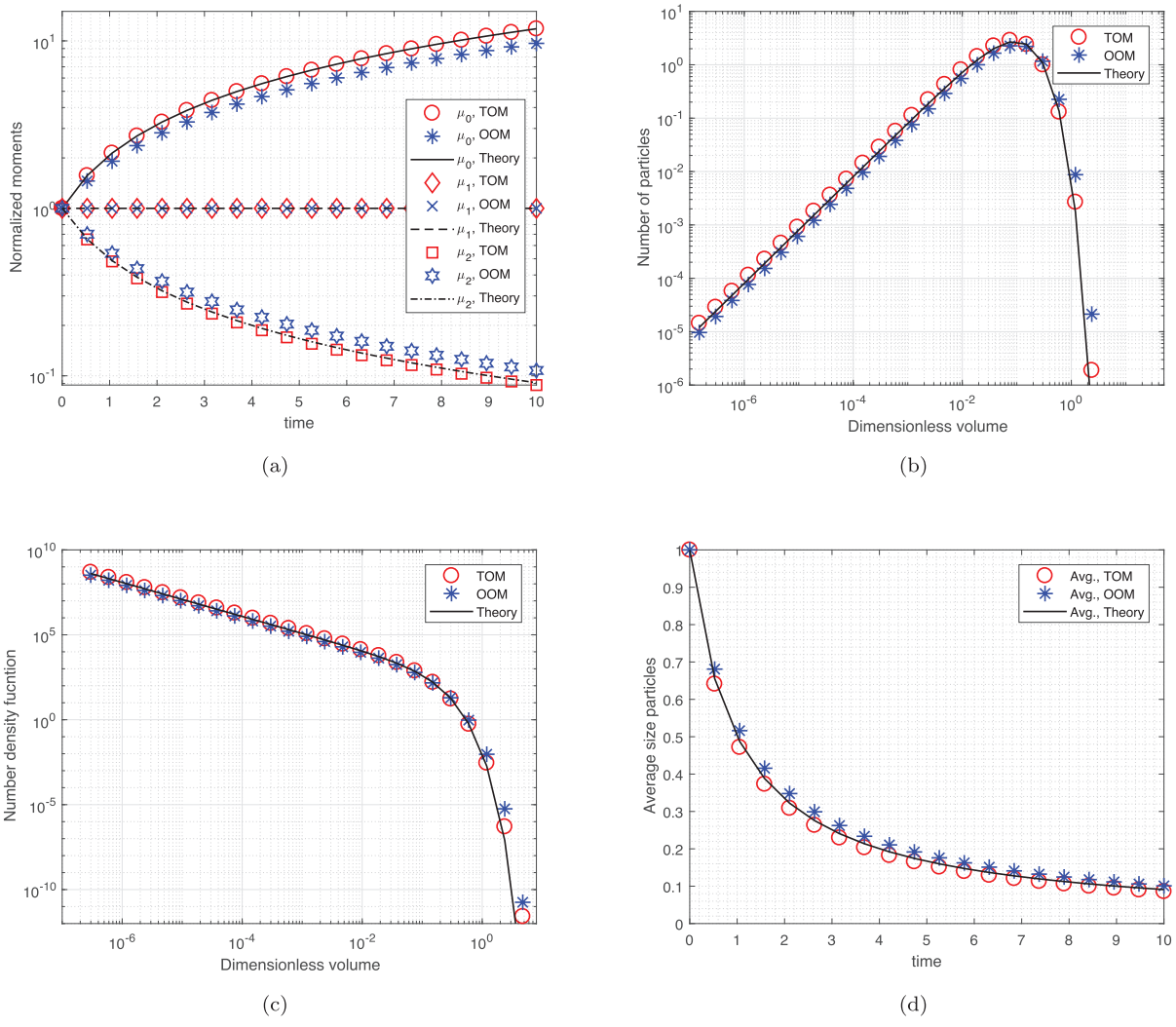

FIGURE 5. Comparison of normalized moments, number of particles, number density function and average particle size using Case 2. (a) Normalized moments. (b) Number of particles. (c) Number density function. (d) Average size particles.

TABLE 2. Weighted sectional errors in the number density function for Test Case 2.

λ	OOM 30 cells	TOM 30 cells	OOM 60 cells	TOM 60 cells
λ_0	0.15338	0.09318	0.04401	0.02398
λ_1	0.15750	0.05709	0.04364	0.01668
λ_2	0.25707	0.05750	0.06626	0.01790

Figure 5a. The particle size distribution (number of particles in each cell) and number density function plotted in Figures 5b and 5c affirm the accuracy of the TOM FVS whereas the OOM FVS shows over prediction for these results. The average size particle obtained in the system is predicted by the TOM FVS with higher precision and agrees well with the theoretical results. However, the OOM FVS shows overprediction for this results as shown in Figure 5d. Additionally, the sectional errors in the number density functions shown in Table 2 acknowledges the accuracy of the TOM FVS over the OOM FVS. One can observe that the sectional errors can be scale down to desired level by considering a more dense grid.

4.3. Test Cases 3 and 4

In this part of the article, the comparison is enhanced by testing the numerical methods against the theoretical results corresponding to Cases 3 and 4. It is worth noting that the theoretical results for the number density functions for these cases are not available in the literature. Therefore, the accuracy of both finite volume approaches are measured by comparing with the theoretical integral moments. The computational domain consists of particle properties ranges from 10^{-9} to 2 is discretized into 30 nonuniform cells. Both numerical methods are run till time $t = 2$ for monodisperse and exponential ICs.

Different order moments are computed with excellent precision by the TOM FVS corresponding to both monodisperse and exponential ICs as shown in Figures 6a and 6c. In addition, the average size of particles formed in the system obtained by the TOM FVS also match well with the theoretical results for both cases (see Figs. 6b and 6d). However, the OOM FVS shows overproduction for these results.

From the above discussion, it can be concluded that the mathematical formulations of both finite volume approaches are very simple and robust to implement of any kind of grid, selection function and breakage kernel. However, the validation exhibits that the TOM FVS is much more accurate in predicting the number density functions, integral moments and average size particles than the OOM FVS. In terms of efficiency, both approaches take almost same computational time to approximate all numerical results.

4.4. Application to depolymerization problem

Now our next aim is to implement these numerical methods real-life application in the area of polymerization sciences [22, 28] in order to check the accuracy of these methods. Chain-end scission problem is solved which in the polymer context refers to the removal of one monomer unit from the end of the polymer chain. Recently, Ahamed *et al.* [1] implemented cell average technique and fixed pivot technique to check their performances for the case of depolymerization on a discrete continuous grid. A standard case of the starch polymer with glucose as the monomer similar to Saito [37] is considered corresponding to the following initial distribution:

$$m(0,u) = \frac{W_0 u n(u)}{\int_1^R [(162u+18)-180]n(u)\mathrm{d}u}, \tag{4.2}$$

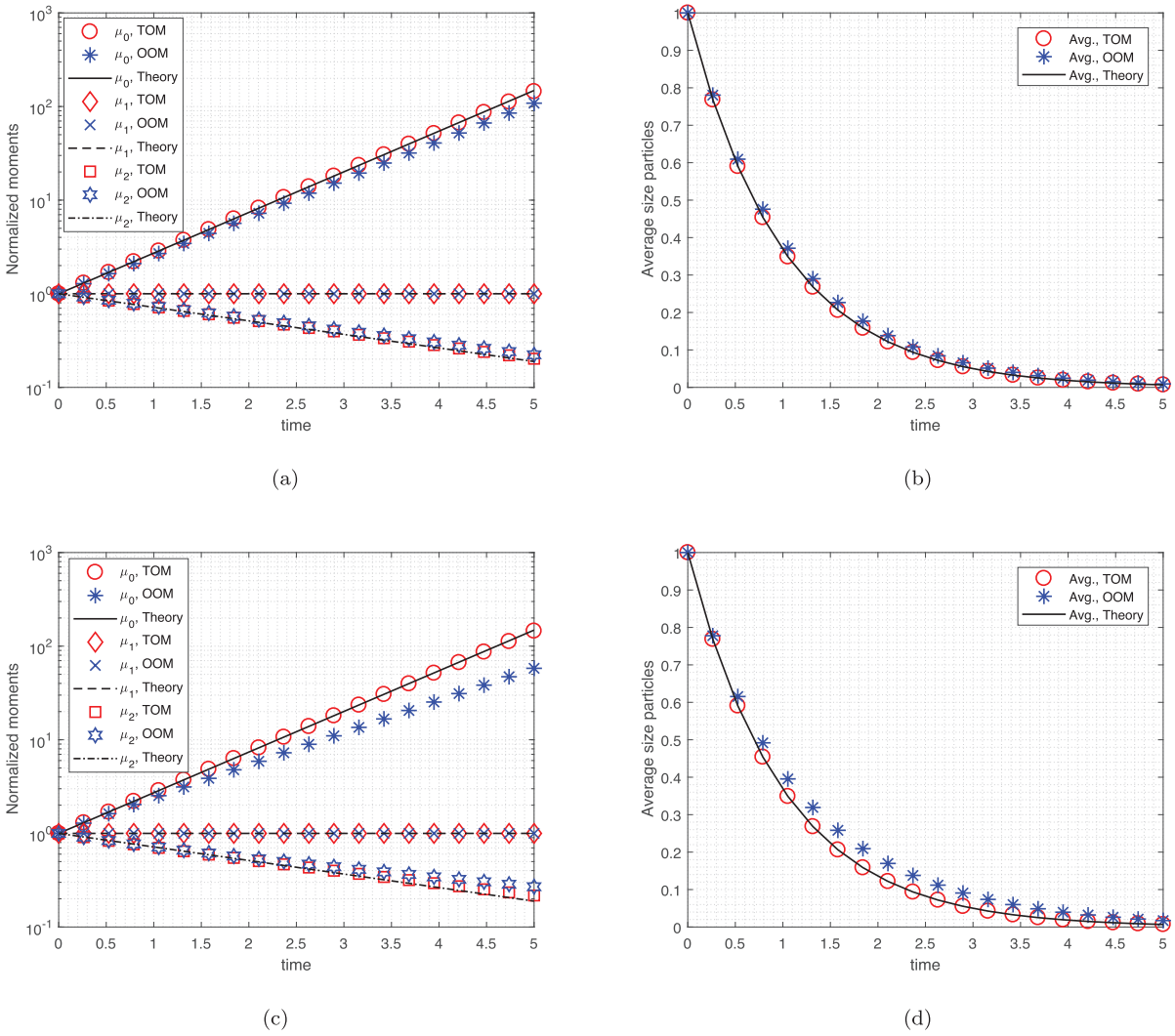

FIGURE 6. Comparison of normalized moments and average size particles using Cases 3 and 4. (a) Normalized moments for exponential IC. (b) Average size particles for exponential IC. (c) Normalized moments for monodisperse IC. (d) Average size particles for monodisperse IC.

where W_0 is the initial mass concentration of the polymer considered and R is the maximum degree of polymerization (DP) of the polymer. The function $n(u)$ is defined as follows:

$$n(u) = \frac{A^{\nu-1}\exp(-A)}{\beta\Gamma(\nu)}, \tag{4.3}$$

where $A = \frac{(u-1)}{\beta}$, $\nu = \frac{W_1}{\beta}$, $\beta = W_2 - W_1$ and $\Gamma(\nu)$ denotes the gamma function. The values of parameters are provided by [10] which are listed here as the number-average DP $W_1 = 4100$, weight-average DP $W_2 = 5430$, $R = 22496$ and $W_0 = 10g/L$. For this case study, a geometric grid with a common ratio of $r = \left[\frac{u_{m+r}}{u_{m+1}}\right]^{\frac{1}{r-1}}$ is used corresponding to $m = 10$ and $r = 30$. Detailed description of the depolymerization problem and knowledge

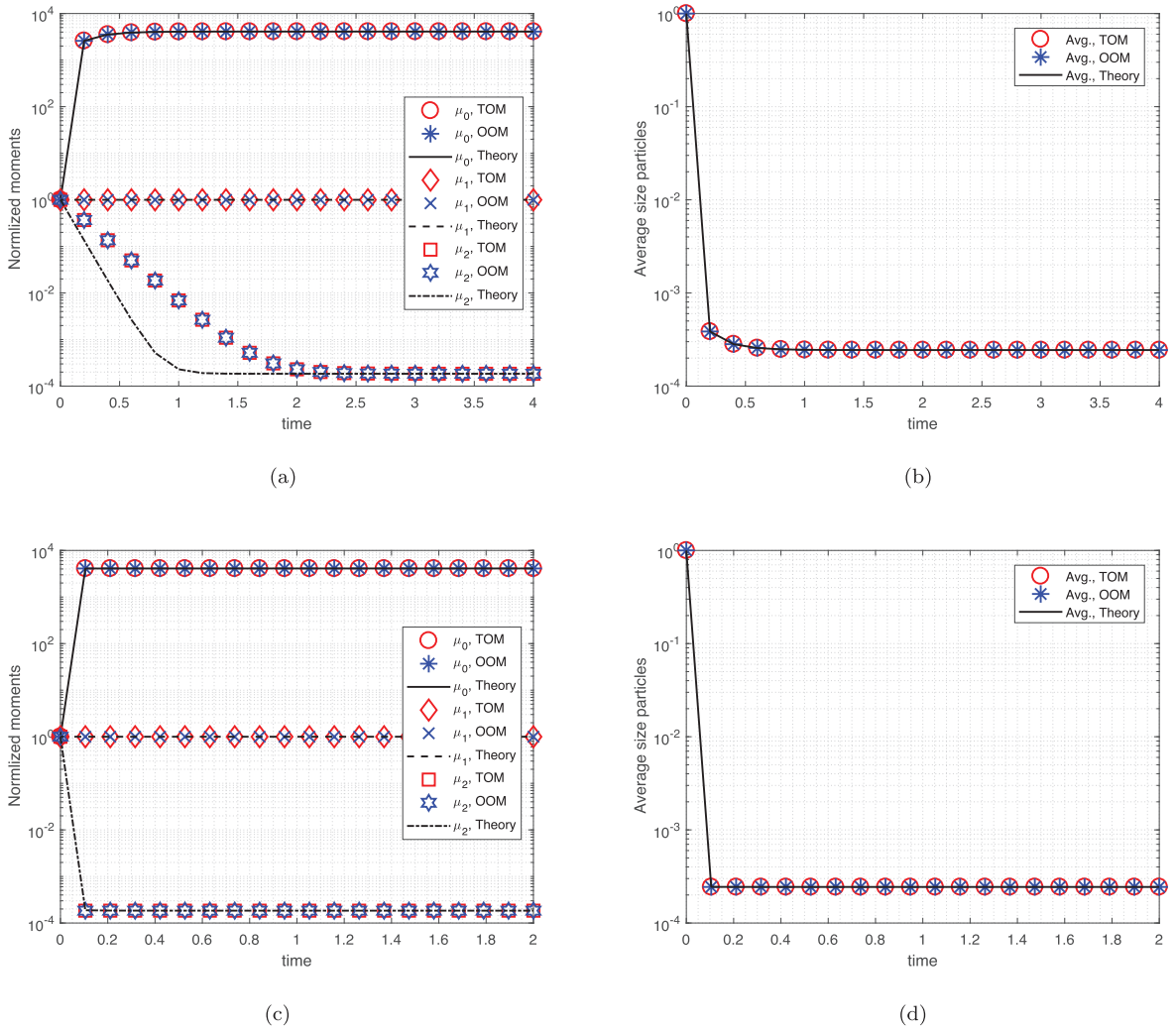

FIGURE 7. Comparison of normalized moments and average size particles for linear and quadratic selection function corresponding to the depolymerization problem. (a) Normalized moments for $S(u) = u$. (b) Average size particles for $S(u) = u$. (c) Normalized moments for $S(u) = u^2$. (d) Average size particles for $S(u) = u^2$.

of the grid can be found in [1]. The numerical results are compared against the theoretical results for linear and quadratic selection functions.

From Figure 7a, it can be seen that the zeroth and first order moments obtained by TOM FVS and OOM FVS are well matched with the theoretical results for linear selection function. The second order moments deviate from the theoretical result, however, the accuracy of this particular moment can be improved by considering a dense grid. Similar to the linear selection function, the zeroth and first order moments obtained by TOM FVS and OOM FVS show equal accuracy and coincide with the theoretical results for a quadratic selection function (see Fig. 7c). In addition, both methods also compute the second order moment with equal precision in contrast to the linear selection function. In both cases, the average size particles are predicted with equal accuracy by the OOM FVS and TOM FVS as both methods match well with the theoretical results (refer to Figs. 7b and 7d).

TABLE 3. Absolute maximum errors in different order moments for quadratic selection function in case of depolymerization problem.

λ	FPT	CAT	OOM	TOM	FPT	CAT	OOM	TOM
		For $m = r = 100$				For $m = 100$, $r = 200$		
λ_0	0.011	0.011	5.10×10^{-4}	2.69×10^{-4}	3.49×10^{-4}	3.49×10^{-4}	1.32×10^{-4}	1.12×10^{-4}
λ_1	0.011	0.011	5.10×10^{-4}	2.69×10^{-4}	3.49×10^{-4}	3.49×10^{-4}	1.32×10^{-4}	1.12×10^{-4}
λ_2	0.011	0.011	5.0×10^{-4}	3.0×10^{-4}	3.49×10^{-4}	3.49×10^{-4}	1.0×10^{-4}	1.0×10^{-4}

TABLE 4. CPU time taken by numerical methods for quadratic selection function in case of depolymerization problem.

Method	Cells	Time taken (in seconds)	Cells	Time taken (in seconds)
FPT	$m = r = 100$	4.8	$m = 100$, $r = 200$	10.9
CAT	$m = r = 100$	9.7	$m = 100$, $r = 200$	18.1
OOM	$m = r = 100$	2.9	$m = 100$, $r = 200$	3.4
TOM	$m = r = 100$	3.5	$m = 100$, $r = 200$	4.7

In order to observe the errors in the moments, the maximum relative order errors (4.4) computed using fixed pivot technique (FPT), cell average technique (CAT), OOM and TOM finite volume schemes are listed in Table 2.

$$\lambda_i(t) = \left| \frac{\mu_i^{\text{theory}}(t) - \mu_i^{\text{num}}(t)}{\mu_i^{\text{theory}}(t)} \right|. \tag{4.4}$$

Here, $\mu_i^{\text{theory}}(t)$ and $\mu_i^{\text{num}}(t)$ denote the values of theoretical and numerical moment at time t, respectively.

It reveals that the FPT and CAT predict these errors with equal accuracy. However, both FPT and CAT show more errors than the OOM FVS and TOM FVS. Moreover, among OOM FVS and TOM FVS, the TOM FVS exhibits more accuracy than the OOM FVS as it computes all integral moments with lesser errors. These errors can be reduced to desired level by adding more grid points in the domain. However, still the TOM performs much better than the other methods. In terms of computational time, both OOM FVS and TOM FVS take lesser CPU time to compute all numerical results as shown in Table 4 whereas other methods consume more computational time than the ROM FVS.

5. CONCLUDING REMARK

In this paper, two finite volume approaches have been proposed for solving a reduced fragmentation models. The first scheme (OOM) focuses on conserving the total mass in the system, however, the second method (TOM) also shows consistency with the zeroth order moment and total mass in the system. Both methods have important features including simple mathematical formulations, easy to code, faster to run and robust to implement on any kind of grid. The formulations have been further supported well by conducting the convergence analysis and show second order convergence for both methods. By testing against theoretical results for various combinations of selection function and binary breakage function, it has been demonstrated that the TOM FVS is more accurate than the OOM FVS. In order to demonstrate the accuracy of both methods, the sectional errors in the number density functions have been estimated and compared. The TOM FVS shows approximately 50%

more accuracy than the OOM FVS. It has been also demonstrated that both proposed numerical methods are second order convergent independently of the kind of discretization used.

Finally, both proposed approaches have been used to solve real-life application well known as chain end depolymerization arises in the area of chemical sciences. The new schemes show equal accuracy in terms of computing the integral moments and average size particles, however, the TOM takes lesser CPU time to approximate all numerical results than the other numerical methods.

Appendix A. Important definitions and theorems for convergence

Now, let us provide some definitions of the errors which will be used in conducting the convergence analysis of the numerical scheme.

Definition A.1. The residual left by substituting the exact solution $\mathbf{m} = [m_1(t), m_2(t), \ldots, m_I(t)]$ in the discrete system of equations is known as spatial truncation error. The mathematical expression for the spatial truncation error is given by

$$\sigma(t) = \frac{\mathrm{d}\mathbf{m}(t)}{\mathrm{d}t} - \mathbf{J}(\mathbf{m}).$$

The numerical scheme is said to be consistent of order p, if $\Delta u \to 0$

$$\|\sigma(t)\| = \mathcal{O}(\Delta u^p), \quad \text{uniformly for all } t,\ 0 \le t \le T.$$

Now, let us define another type of discretization error which will be used to find the order of convergence.

Definition A.2. The global discretization error for the numerical scheme is the difference between the exact and numerical solution $\epsilon(t) = m(t) - \hat{m}(t)$. The numerical scheme is said to be convergent of order p if, for $\Delta u \to 0$,

$$\|\epsilon(t)\| = \mathcal{O}(\Delta u^p), \quad \text{uniformly for all } t,\ 0 \le t \le T. \tag{A.1}$$

At this point of time, let us state the theorem for the convergence of the numerical scheme.

Theorem A.3. *Let us consider that* $\boldsymbol{J}$ *is continuous and satisfies the Lipschitz condition*

$$\|\boldsymbol{J(m)} - \boldsymbol{J}(\hat{\boldsymbol{m}})\| \le C\|\boldsymbol{m} - \hat{\boldsymbol{m}}\| \text{ for all } \boldsymbol{m}, \hat{\boldsymbol{m}} \in \mathbb{R}^I,\ C < \infty. \tag{A.2}$$

Then the solution of semidiscrete system $\boldsymbol{m}' = \boldsymbol{J(m)}$ *is non-negative iff for any vector* $\boldsymbol{m} \in \mathbb{R}^I$ *and all* $i = 1, 2, \ldots, I$, *and* $t \ge 0$,

$$\boldsymbol{m} \ge 0, \quad m_i = 0 \Rightarrow J_i(\boldsymbol{m}) \ge 0.$$

Proof. The generalized proof of the above theorem can be seen in [15] (Thm. 7.1 in Chap. 1). □

Theorem A.4. *Let us suppose that a Lipschitz condition on* $\mathbf{J}(\mathbf{m})$ *is satisfied for* $0 \le t \le T$ *and for all* $m, \hat{m} \in \mathbb{R}^I$. *That is,* $\mathbf{J}$ *satisfies*

$$\|\mathbf{J}(\mathbf{m}) - \mathbf{J}(\hat{\mathbf{m}})\| \le L\|\mathbf{m} - \hat{\mathbf{m}}\|, \quad L < \infty. \tag{A.3}$$

Then a consistent discretization scheme is also convergent and the convergent order is the same as the order of consistency.

Proof. The detailed proof of this theorem is given in [26]. □

Acknowledgements. The authors gratefully acknowledge the financial support provided by EU H2020 Marie Skłodowska-Curie Individual Fellowship no. 841906 to Dr. Mehakpreet Singh.

References

[1] F. Ahamed, M. Singh, H.-S. Song, P. Doshi, C.W. Ooi and Y.K. Ho, On the use of sectional techniques for the solution of depolymerization population balances: Results on a discrete-continuous mesh. *Adv. Powder Technol.* **31** (2020) 2669–2679.

[2] H. Amann and C. Walker, Local and global strong solutions to continuous coagulation–fragmentation equations with diffusion. *J. Differ. Equ.* **218** (2005) 159–186.

[3] L.G. Austin, Introduction to the mathematical description of grinding as a rate process. *Powder Technol.* **5** (1971) 1–17.

[4] G. Baird and E. Süli, A finite volume scheme for the solution of a mixed discrete-continuous fragmentation model. *ESAIM: M2AN* **55** (2021) 1067–1101.

[5] E. Ben-Naim and P. Krapivsky, Multiscaling in fragmentation. *Phys. D: Nonlinear Phenom.* **107** (1997) 156–160.

[6] E. Bilgili and B. Scarlett, Population balance modeling of non-linear effects in milling processes. *Powder Technol.* **153** (2005) 59–71.

[7] M. Bonacini, B. Niethammer and J.J. Velázquez, Solutions with peaks for a coagulation–fragmentation equation. Part I: stability of the tails. *Commun. Partial. Differ. Equ.* **45** (2020) 351–391.

[8] J.-P. Bourgade and F. Filbet, Convergence of a finite volume scheme for coagulation-fragmentation equations. *Math. Comput.* **77** (2008) 851–882.

[9] D. Boyer, G. Tarjus and P. Viot, Exact solution and multifractal analysis of a multivariable fragmentation model. *J. Phys. I* **7** (1997) 13–38.

[10] W. Breuninger, K. Piyachomkwan and K. Sriroth, Chapter 12-tapioca/cassava starch: production and use. Starch (Third Edition) 1 (2009) 541–568.

[11] J. Calvo and P.-E. Jabin, Large time asymptotics for a modified coagulation model. *J. Differ. Equ.* **250** (2011) 2807–2837.

[12] J.A. Cañizo and S. Throm, The scaling hypothesis for smoluchowski's coagulation equation with bounded perturbations of the constant kernel. *J. Differ. Equ.* **270** (2021) 285–342.

[13] M. Escobedo, P. Laurençot, S. Mischler and B. Perthame, Gelation and mass conservation in coagulation-fragmentation models. *J. Differ. Equ.* **195** (2003) 143–174.

[14] M. Hounslow, J. Pearson and T. Instone, Tracer studies of high-shear granulation: II. Population balance modeling. *AIChE J.* **47** (2001) 1984–1999.

[15] W. Hundsdorfer and J.G. Verwer, Numerical solution of time-dependent advection-diffusion-reaction equations. Vol. 33. Springer Science & Business Media (2013).

[16] H.Y. Ismail, S. Shirazian, M. Singh, D. Whitaker, A.B. Albadarin and G.M. Walker, Compartmental approach for modelling twin-screw granulation using population balances. *Int. J. Pharm.* **576** (2020) 118737.

[17] H.Y. Ismail, M. Singh, S. Shirazian, A.B. Albadarin and G.M. Walker, Development of high-performance hybrid ann-finite volume scheme (ann-fvs) for simulation of pharmaceutical continuous granulation. *Chem. Eng. Res. Des.* **163** (2020) 320–326.

[18] P. Kapur and P. Agrawal, Approximate solutions to the discretized batch grinding equation. *Chem. Eng. Sci.* **25** (1970) 1111–1113.

[19] G. Kaur, M. Singh, J. Kumar, T. De Beer and I. Nopens, Mathematical modelling and simulation of a spray fluidized bed granulator. *Processes* **6** (2018) 195.

[20] G. Kaur, M. Singh, T. Matsoukas, J. Kumar, T. De Beer and I. Nopens, Two-compartment modeling and dynamics of top-sprayed fluidized bed granulator. *Appl. Math. Model.* **68** (2019) 267–280.

[21] G. Kaur, R. Singh, M. Singh, J. Kumar and T. Matsoukas, Analytical approach for solving population balances: a homotopy perturbation method. *J. Phys. A: Math. Theor.* **52** (2019) 385201.

[22] M. Kostoglou, Mathematical analysis of polymer degradation with chain-end scission. *Chem. Eng. Sci.* **55** (2000) 2507–2513.

[23] J. Kumar, M. Peglow, G. Warnecke, S. Heinrich and L. Mörl, A discretized model for tracer population balance equation: Improved accuracy and convergence. *Comput. Chem. Eng.* **30** (2006) 1278–1292.

[24] R. Kumar, J. Kumar and G. Warnecke, Moment preserving finite volume schemes for solving population balance equations incorporating aggregation, breakage, growth and source terms. *Math. Models Methods Appl. Sci.* **23** (2013) 1235–1273.

[25] C. Lécot and W. Wagner, A quasi–monte carlo scheme for smoluchowski's coagulation equation. *Math. Comput.* **73** (2004) 1953–1966.

[26] P. Linz, Convergence of a discretization method for integro-differential equations. Numerische Mathematik **25** (1975) 103–107.

[27] H. Liu and M. Li, Two-compartmental population balance modeling of a pulsed spray fluidized bed granulation based on computational fluid dynamics (cfd) analysis. *Int. J. Pharm.* **475** (2014) 256–269.

[28] B.J. McCoy and G. Madras, Discrete and continuous models for polymerization and depolymerization. *Chem. Eng. Sci.* **56** (2001) 2831–2836.

[29] D. McLaughlin, W. Lamb and A. McBride, An existence and uniqueness result for a coagulation and multiple-fragmentation equation. *SIAM J. Math. Anal.* **28** (1997) 1173–1190.

[30] D. McLaughlin, W. Lamb and A. McBride, A semigroup approach to fragmentation models. *SIAM J. Math. Anal.* **28** (1997) 1158–1172.

[31] M.N. Nandanwar and S. Kumar, A new discretization of space for the solution of multi-dimensional population balance equations: Simultaneous breakup and aggregation of particles. *Chem. Eng. Sci.* **63** (2008) 3988–3997.

[32] H.M. Omar and S. Rohani, Crystal population balance formulation and solution methods: A review. *Cryst. Growth Des.* **17** (2017) 4028–4041.

[33] M. Peglow, J. Kumar, G. Warnecke, S. Heinrich, E. Tsotsas, L. Mörl and M. Hounslow, An improved discretized tracer mass distribution of Hounslow et al. *AIChE J.* **52** 1326–1332.
[34] C.L. Prasher, Crushing and grinding process handbook. Wiley (1987).
[35] K.J. Reid, A solution to the batch grinding equation. *Chem. Eng. Sci.* **20** (1965) 953–963.
[36] F. Rezakhanlou, Moment bounds for the solutions of the smoluchowski equation with coagulation and fragmentation. *Proc. R. Soc. Edinb. A: Math.* **140** (2010) 1041–1059.
[37] O. Saito, Statistical theories of cross-linking. The radiation chemistry of macromolecules 1 (1972) 223.
[38] S. Shirazian, H.Y. Ismail, M. Singh, R. Shaikh, D.M. Croker, G.M. Walker, Multi-dimensional population balance modelling of pharmaceutical formulations for continuous twin-screw wet granulation: Determination of liquid distribution. *Int. J. Pharm.* **566** (2019) 352–360.
[39] M. Singh, Accurate and efficient approximations for generalized population balances incorporating coagulation and fragmentation. *J. Comput. Phys.* **435** (2021) 110215.
[40] P. Singh and M. Hassan, Kinetics of multidimensional fragmentation. *Phys. Rev. E* **53** (1996) 3134.
[41] M. Singh and G. Walker, Finite volume approach for fragmentation equation and its mathematical analysis. *Numer. Algorithms* **89** (2021) 465–486.
[42] M. Singh, G. Kaur, T. De Beer and I. Nopens, Solution of bivariate aggregation population balance equation: a comparative study. *React. Kinet. Mech. Catal.* **123** (2018) 385–401.
[43] M. Singh, T. Matsoukas, A.B. Albadarin, G. Walker, New volume consistent approximation for binary breakage population balance equation and its convergence analysis. *ESAIM: M2AN* **53** (2019) 1695–1713.
[44] M. Singh, K. Vuik, G. Kaur and H.-J. Bart, Effect of different discretizations on the numerical solution of 2d aggregation population balance equation. *Powder Technol.* **342** (2019) 972–984.
[45] M. Singh, T. Matsoukas and G. Walker, Two moments consistent discrete formulation for binary breakage population balance equation and its convergence. *Appl. Numer. Math.* **166** (2021) 76–91.
[46] E. Teunou and D. Poncelet, Batch and continuous fluid bed coating–review and state of the art. *J. Food Eng.* **53** (2002) 325–340.
[47] A. Vreman, C. Van Lare and M. Hounslow, A basic population balance model for fluid bed spray granulation. *Chem. Eng. Sci.* **64** (2009) 4389–4398.
[48] R.M. Ziff, New solutions to the fragmentation equation. *J. Phys. A: Math. General* **24** (1991) 2821.
[49] R.M. Ziff and E. McGrady, The kinetics of cluster fragmentation and depolymerisation. *J. Phys. A: Math. General* **18** (1985) 3027.